Title: The high-production volume fungicide pyraclostrobin induces triglyceride accumulation associated with mitochondrial dysfunction, and promotes adipocyte differentiation independent of PPARγ activation, in 3T3-L1 cells

Authors: Anthony L. Luz, Christopher D. Kassotis, Heather M. Stapleton, Joel N. Meyer

PII: S0300-483X(17)30340-2
DOI: https://doi.org/10.1016/j.tox.2017.11.010
Reference: TOX 51978

To appear in: *Toxicology*

Received date: 9-10-2017
Revised date: 27-10-2017
Accepted date: 6-11-2017

Please cite this article as: Luz, Anthony L., Kassotis, Christopher D., Stapleton, Heather M., Meyer, Joel N., The high-production volume fungicide pyraclostrobin induces triglyceride accumulation associated with mitochondrial dysfunction, and promotes adipocyte differentiation independent of PPARγ activation, in 3T3-L1 cells.Toxicology https://doi.org/10.1016/j.tox.2017.11.010

The high-production volume fungicide pyraclostrobin induces triglyceride accumulation associated with mitochondrial dysfunction, and promotes adipocyte differentiation independent of PPARγ activation, in 3T3-L1 cells

Anthony L. Luz[*], Christopher D. Kassotis[*], Heather M. Stapleton[*], Joel N. Meyer[*,†]

[*]Nicholas School of the Environment, Box 90328, Duke University, Durham, NC, USA, 27708

[†]Author to whom correspondence and reprint requests should be addressed.

anthony.luz@duke.edu

christopher.kassotis@duke.edu

heather.stapleton@duke.edu

joel.meyer@duke.edu

Abstract

Pyraclostrobin is one of the most heavily used fungicides, and has been detected on a variety of produce, suggesting human exposure occurs regularly. Recently, pyraclostrobin exposure has been linked to a variety of toxic effects, including neurodegeneration and triglyceride (TG) accumulation. As pyraclostrobin inhibits electron transport chain complex III, and as mitochondrial dysfunction is associated with metabolic syndrome (cardiovascular disease, type II diabetes, obesity), we designed experiments to test the hypothesis that mitochondrial dysfunction underlies its adipogenic activity. 3T3-L1 cells were differentiated according to standard protocols in the presence of pyraclostrobin, resulting in TG accumulation. However, TG accumulation occurred without activation of the peroxisome proliferator activated nuclear receptor gamma (PPARγ), the canonical pathway mediating adipogenesis. Furthermore, cells failed to express many markers of adipogenesis (*PPARγ, lpl, CEBPα*), while co-exposure to pyraclostrobin and two different PPARγ antagonists (GW9662, T0070907) failed to mitigate TG accumulation, suggesting TG accumulation occurred through a PPARγ-independent mechanism. Instead, pyraclostrobin reduced steady-state ATP, mitochondrial membrane potential, basal mitochondrial respiration, ATP-linked respiration, and spare respiratory capacity, demonstrating mitochondrial dysfunction, while reduced expression of genes involved in glucose transport (*Glut-4*), glycolysis (*Pkm*, *Pfkl*, *Pfkm*), fatty acid oxidation (*Cpt-1b*), and lipogenesis (*Fasn*, *Acacα, Acacβ*) further suggested a disruption of metabolism. Finally, inhibition of cAMP responsive element binding protein (CREB), a PPARγ coactivator, partially mitigated pyraclostrobin-induced TG accumulation, suggesting TG accumulation is occurring through a CREB-driven mechanism. In contrast, rosiglitazone, a known PPARγ agonist, induced TG

accumulation in a PPARγ-dependent manner and enhanced mitochondrial function. Collectively, these results suggest pyraclostrobin-induced mitochondrial dysfunction inhibits lipid homeostasis, resulting in TG accumulation. Exposures that disrupt mitochondrial function may have the potential to contribute to the rising incidence of metabolic syndrome, and thus more research is needed to understand the human health impact of pyraclostrobin exposure.

Key words: Pyraclostrobin; Fungicide; Adipogenesis; Mitochondrial toxicity; Metabolic disruption

1. Introduction

Globally, the incidence of metabolic syndrome, which includes cardiovascular disease, type II diabetes, and obesity, has increased dramatically. Over the past several decades the rate of obesity in U.S. adults has increased from 13 to 35% (Ogden *et al.*, 2014), while the rate of type II diabetes in U.S. adolescents has increased by around 30% (Dabelea *et al.*, 2014), and thus represents a significant socio-economic burden (Hammond and Levine, 2010). However, the rising incidence of metabolic syndrome is not limited to developed countries, as rates of cardiovascular disease, type II diabetes, and obesity have dramatically increased (up to 10-fold) in sub-Saharan Africa over the past two decades (Amuna and Zotor, 2008). Thus, the rising incidence of metabolic syndrome represents an important global health burden.

Emerging evidence has implicated mitochondrial dysfunction in numerous metabolic disorders, including obesity (Heilbronn *et al.*, 2007; Semple *et al.*, 2004), types I and II diabetes (Lowell and Shulman, 2005; Petersen *et al.*, 2003), and lipodystrophy in HIV-patients treated with highly active anti-retroviral therapy, a therapy associated with mitochondrial dysfunction

(Falutz, 2007). Interestingly, many of the same transcription factors that regulate adipogenesis and triglyceride (TG) accumulation also regulate mitochondrial biogenesis. For example, the peroxisome proliferator activated nuclear receptor gamma (PPARγ), cAMP responsive element binding protein (CREB), and CCAT/enhancer-binding protein (C/EBP) family members control the transcription of numerous genes involved in adipogenesis and TG accumulation [reviewed in (Tang and Lane, 2012)]. However, transcriptional regulation typically requires the participation of PPARγ coactivator 1 (PGC-1), in a process that engages both adipogenesis and mitochondrial biogenesis (Spiegelman *et al.*, 2000). Coordination of these processes is further demonstrated by the fact that rosiglitazone, a potent PPARγ agonist, synchronously induces adipogenesis and TG accumulation, as well as increases mitochondrial protein expression and mitochondrial oxygen consumption. This increase in mitochondrial biogenesis is believed to be required for cells to meet the rising energy demands associated with lipogenesis (Wilson-Fritch *et al.*, 2003; Wilson-Fritch *et al.*, 2004). Furthermore, mitochondrial metabolism is required for both lipogenesis and lipolysis. Mitochondrial-derived acetyl-CoA and glycerol-3-phosphate (derived via glycolysis or glyceroneogenesis) serve as TG precursors required for lipogenesis, while free fatty acids derived from lipolysis undergo fatty acid oxidation in the mitochondrial matrix to fuel the Krebs cycle. The critical role of mitochondria in maintaining lipid homeostasis is further demonstrated by the fact that exposure to mitochondrial uncouplers or electron transport chain (ETC) inhibitors, which deplete ATP, result in an inhibition of lipolysis, which is believed to be mediated by AMP-activated protein kinase, a molecular sensor of energetic stress (Daval *et al.*, 2005; Fassina *et al.*, 1974).

Given the numerous links between mitochondrial health, adipogenesis, and lipid homeostasis, it is not surprising that mitochondrial dysfunction has been implicated in metabolic

and fat storage disorders. Interestingly, exposure to several prototypical electron transport chain (ETC) inhibitors, including rotenone (complex I (CI)), antimycin A (complex III (CIII)), and oligomycin (ATP synthase/complex V (CV)), have been shown to induce TG accumulation in 3T3-L1 cells (Vankoningsloo *et al.*, 2006; Vankoningsloo *et al.*, 2005). However, the human health relevance of these compounds is limited. Alternatively, pyraclostrobin, and other members of the strobilurin class of fungicides, which inhibit ETC CIII activity (Becker *et al.*, 1981) can also induce TG accumulation in murine (Kassotis *et al.*, 2017a) and human (Foley *et al.*, 2017) *in vitro* models of adipogenesis. Since its introduction to the market in 2003, pyraclostrobin has rapidly become one of the most heavily used agricultural fungicides, with $735 million in sales in 2009 (Oliver and Hewitt, 2014), and over two million pounds of pyraclostrobin applied to U.S. crops in 2014 (USGS, 2017). Despite a relatively short environmental half-life (1-4 days) (Li *et al.*, 2010; You *et al.*, 2012; Zhang *et al.*, 2009), pyraclostrobin has been detected (in the ppm range in some cases) on a variety of fruits and vegetables (Dong *et al.*, 2012; Guo *et al.*, 2017; Kovacova *et al.*, 2013; Pearson *et al.*, 2016) and in streams (Battaglin *et al.*, 2011). Furthermore, rinsing pyraclostrobin-treated produce with tap water only removes 18-30% of the fungicide, even with extensive rinsing (~5 minutes) (Lozowicka and Jankowska, 2016; Lozowicka *et al.*, 2016). Given the high volume of pyraclostrobin in use, frequent detection on fruits and vegetables, and its inability to be efficiently removed from produce via traditional rinsing methods, human exposure to pyraclostrobin is probable; however, very little human exposure data is available.

Given the high potential for human exposure, the link between mitochondrial dysfunction and metabolic syndrome, and the fact that pyraclostrobin has previously been shown to induce TG accumulation in 3T3-L1 cells, we set out to test the hypothesis that mitochondrial

dysfunction is associated with TG accumulation in 3T3-L1 cells, a well validated model of adipogenesis frequently used for screening chemicals for adipogenic activity (Kassotis *et al.*, 2017a; Kassotis *et al.*, 2017b), continuously exposed to the fungicide pyraclostrobin.

2. Materials and Methods

2.1 Cell Culture Conditions

3T3-L1 cells were obtained from Zenbio, Inc. at passage 8 (Cat. # SP-L1-F, lot # 3T3062104; Research Triangle Park, NC) and were maintained as described previously in pre-adipocyte maintenance media (Dulbecco's Modified Eagle Medium – High Glucose (DMEM-HG; Gibco # 11995), 10% BCS, 1% penicillin and streptomycin (Pen-Strep; Gibco # 15140)) (Kassotis *et al.*, 2017a; Kassotis *et al.*, 2017b). Cells were maintained in a sub-confluent state until differentiation and each thaw of frozen cells was utilized within 6 passages, with no significant changes in control chemical response observed in that time. HEK 293H cells utilized for the GeneBlazer™ PPARγ assays (Invitrogen # K1094) were cultured in DMEM-HG supplemented with 10% fetal bovine serum (FBS, Invitrogen # 26400-036), 1% non-essential amino acids (Invitrogen # 11140), 1% sodium pyruvate (Invitrogen # 11360), 1% Pen-Strep, 1 M HEPES (Invitrogen # 15630), 80 µg/ml hygromycin (Invitrogen # 10687), 1% glutamax (Invitrogen # 35050), and 500 µg/ml Geneticin (Invitrogen # 10131). Each thaw of HEK 293H cells was maintained in a sub-confluent state and utilized for assays within 10 passages.

2.3 3T3-L1 Differentiation

3T3-L1 Cells were induced to differentiate as described previously (Kassotis *et al.*, 2017a; Kassotis *et al.*, 2017b). Briefly, cells were seeded in pre-adipocyte media into 96-well tissue culture plates (Greiner # 655090) at approximately 30,000 cells per well. Once confluent, cells were cultured for an additional 2 days to promote growth arrest and allow initiation of

clonal expansion. Media was then replaced with test chemicals and/or controls using a 0.1% DMSO vehicle in differentiation media (DMEM-HG with 10% FBS, 1% Pen-Strep, 1.0 µg/ml human insulin, and 0.5 mM 3-isobutyl-1-methylxanthine, IBMX). After 2 days, media was replaced with test chemicals diluted in adipocyte maintenance media (differentiation media without IBMX) and these treatments were refreshed every 2 days until plates were assayed.

2.3 DNA and Triglyceride Content

Plates were assayed for TG accumulation and DNA content after 10 days of differentiation as described previously (Kassotis *et al.*, 2017a; Kassotis *et al.*, 2017b). Briefly, media was removed and cells rinsed with Dulbecco's phosphate-buffered saline (DPBS; Gibco # 14040) before replacing with 200 µl/well of a dye mixture (19.5 ml DPBS, 1 drop/mL NucBlue® Live ReadyProbes® Reagent (Thermo # R37605) and 500 µl AdipoRed™ (Lonza # PT-7009) per plate). Plates were incubated at room temperature for approximately 40 minutes, protected from light, and were then read using a Molecular Devices SpectraMax M5 fluorimeter (AdipoRed ($485_{ex}/572_{em}$), NucBlue ($360_{ex}/460_{em}$)). DNA and TG content was calculated as percent change from vehicle control for each chemical at each concentration, and was used to normalize total TG values to obtain TG content per cell.

2.4 3T3-L1 Cell Fluorescence Imaging

Cells were seeded into 24-well plates at approximately 130,000 cells per well and differentiated as described above. After 10 days of differentiation, media was removed, cells were rinsed, and 1 ml of the dye mixture (above) was added to each well. Plates were covered in foil and incubated for 30 minutes before imaging using a Zeiss Axio Observer microscope equipped with a Photometrics CoolSNAP ES2 CCD camera. Imaging was performed using a

10x/0.30 Plan-NeoFluor Ph1 objective, merging the phase contrast (phase1) field with yellow fluorescent protein (Nile red lipid staining) and DAPI (DNA content) filters.

2.5 LDH Release

Cell viability was assessed using the CytoTox-ONE™ assay (Promega # G7890), per slightly amended manufacturer's instructions. A detailed description of this method is provided in the Supplemental Materials and Methods file.

2.6 PPARγ GeneBLAzer™ Reporter Assay

PPARγ agonism was measured according to manufacturer's instructions and as described previously (Fang *et al.*, 2015). Briefly, cells were seeded at approximately 30,000 cells per well into duplicate 384-well black clear-bottom plates (VWR # 62406-352) and allowed to settle for 2-4 hours. Cells were then induced with test chemical and positive/negative controls (0.1 nM – 1 μM rosiglitazone for PPARγ), using a 0.1% DMSO vehicle (identical treatments for duplicate plates). Cells were incubated for approximately 16 hours and then 1 plate each was assayed for receptor activity and cell viability. Receptor activity was assessed using the LiveBLAzer™-FRET B/G Loading Kit (Invitrogen # K1030), adding reagents per manufacturer's instructions, incubating at room temperature for 2 hours, protected from light, and then measuring fluorescence at $409_{ex}/460_{em}$ and $409_{ex}/530_{em}$ on a Molecular Devices SpectraMax M5 fluorimeter. Percent activity was assessed as a background corrected fold induction of test chemical response relative to maximal rosiglitazone-induced response. Cell viability was assessed as described previously (Fang *et al.*, 2015), adding 0.025 mg/mL resazurin solution to each well of the duplicate plate, incubating at 37°C for 2 hours, and then measuring fluorescence at 560/590 nm using the SpectraMax fluorimeter. Cell viability loss of greater than 15% was used as a cut-off for distinguishing significant viability loss and putative cytotoxicity.

2.7 Real-Time PCR-Based Determination of mRNA Expression

Total RNA was isolated from cells using the RNeasy mini kit (Qiagen # 74104) and quantified using a NanoDrop 8000 spectrophotometer (Thermo Scientific). 250 ng of isolated RNA was converted to cDNA using the Omniscript reverse transcription kit (Qiagen # 205111). Real-Time PCR (RT-PCR) was performed using Power SYBR Green Master Mix (ThermoFisher # 4368577) in a 7300 Real-time PCR System (Applied Biosystems). RT-PCR reactions were run with 4ng input cDNA. All RT-PCR primers, annealing temperatures, and amplicon sizes are reported in Supplemental Table 1. The $\log_2$ fold-change in expression of each gene was calculated by comparing the cycle threshold (C_t) of the target gene to the C_t of the house keeping genes (*B2m, Rn18s*) using the $\Delta\Delta C_t$ method. Samples were run in triplicate from 2 separate experiments.

2.8 Mitochondrial Membrane Potential

Mitochondrial membrane potential was determined using the fluorometric dye JC-1. A detailed description of this method is provided in the Supplemental Materials and Methods file.

2.8 Seahorse XF^{e}24 Analysis of Mitochondrial Respiration

The fundamental parameters of mitochondrial respiration (basal oxygen consumption rate (OCR), ATP-linked respiration, maximal OCR, spare respiratory capacity, proton leak) and glycolysis (extracellular acidification rate (ECAR)) were determined using the Seahorse XF^{e}24 Extracellular Flux Analyzer. 3T3-L1 cells were cultured, differentiated, and exposed to chemicals in Seahorse XF24 V7 PS Cell Culture Microplates (Agilent # 100777). Following exposure, media was aspirated, and cells were rinsed twice with unbuffered Seahorse base media (Agilent # 102353) supplemented with D-glucose (4.5 g/L), pyruvate (110 mg/L), and glutamine (584 mg/L), pH 7.4. Cells were then incubated without CO_2 at 37°C for 1 hour prior to analysis.

Mitochondrial respiration was calculated following the sequential injection of 1 µM oligomycin A (CV inhibitor, dissolved in 0.1% DMSO), 2 µM FCCP (mitochondrial uncoupler, dissolved in 0.1% DMSO), and 0.5 µM rotenone and antimycin A (CI and CIII inhibitors, respectively; dissolved in 0.1% ethanol). Three basal OCR measurements were taken prior to oligomycin injection, while an additional 3 OCR measurements were taken after injection of each drug. The fundamental parameters of mitochondrial respiration were then calculated per manufacturer's instructions. Seahorse XF^e experiments were repeated 3 separate times.

2.9 Statistics

Statistical analysis was performed using JMP v11.0 software (SAS Institute). Data was initially analyzed via 1 factor analysis of variance, and when warranted (ANOVA $p<0.05$) post-hoc comparisons to the differentiated, vehicle treated control cells were performed using Dunnett's test or Tukey's HSD. The post-hoc test, N, and p-values for each experiment are provided in the figure legends.

3. Results

3.1 Pyraclostrobin induces triglyceride accumulation.

As previously reported (Kassotis *et al.*, 2017a), continuous exposure to pyraclostrobin (1.0 and 10.0 µM) and rosiglitazone (0.1 and 1.0 µM) throughout a ten-day differentiation window increased 3T3-L1 cell proliferation and TG accumulation in a dose-dependent manner (Fig. S1A-B). Importantly, TG accumulation could not be explained by increased cell proliferation, as normalizing to cell number gave similar results (Fig. S1C). Although rosiglitazone and pyraclostrobin induced similar magnitudes of TG accumulation, the size and abundance of cytosolic TG vesicles varied greatly between the two exposures. Specifically, TG vesicles appeared smaller and more abundant in cells differentiated in the presence of

pyraclostobin, when compared to cells treated with rosiglitazone (Fig. 1). Importantly, continuous exposure to pyraclostrobin for 10-days did not induce LDH release at any concentration, suggesting no reduction in cell viability (Fig. S1D), a finding also recently reported in a human adipose-derived stem cell model of adipogenesis (Foley *et al.*, 2017).

3.2 Pyraclostrobin-induced TG accumulation is independent of PPARγ activation.

Due to the importance of PPARγ in differentiation (Barak *et al.*, 1999; Kubota *et al.*, 1999; Rosen *et al.*, 1999), we first tested the ability of rosiglitazone and pyraclostrobin to act as PPARγ agonists. As expected, rosiglitazone, a well-known PPARγ agonist (Forman *et al.*, 1995; Lehmann *et al.*, 1995), increased PPARγ activity in our reporter assay and mRNA expression in a dose-dependent manner (Fig. 2A-B). Alternatively, pyraclostrobin reduced *PPARγ* mRNA expression, and had no effect on PPARγ activity in our reporter assay (Fig. 2A-B). Furthermore, exposure to pyraclostrobin reduced expression of CCAAT/ enhancer binding protein alpha (*Cebpα*) (Fig. 2C), a transcription factor that works in concert with PPARγ to regulate the expression of genes required for adipogenesis (Lefterova *et al.*, 2008), and lipoprotein lipase (*Lpl*) (Fig. 2D), a gene that is transcriptionally regulated by PPARγ (Schoonjans *et al.*, 1996), while mRNA expression of both *Cebpα* and *Lpl* was induced by rosiglitazone in a dose-dependent manner (Fig. 2C-D). Finally, we co-exposed 3T3-L1 cells to pyraclostrobin or rosiglitazone and several different PPARγ antagonists (GW9662 and T0070907). As expected, both PPARγ antagonists partially mitigated rosiglitazone-induced TG accumulation, while neither antagonist effected pyraclostrobin-induced TG accumulation (Fig 2E). Collectively, these results suggest that pyraclostrobin is inducing TG accumulation through a mechanism independent of PPARγ activity, while also preventing differentiation.

3.4 Pyraclostrobin disrupts mitochondrial energy metabolism.

As previously reported (Kassotis *et al.*, 2017a), continuous exposure to pyraclostrobin throughout a ten-day differentiation window resulted in a dose-dependent reduction in steady-state ATP levels (Fig. 3A), suggesting a disruption of mitochondrial function. To further test the effects of pyraclostrobin on mitochondrial function under these conditions, we assessed mitochondrial respiration using the Seahorse XF^e Bioanalyzer. Exposure to 0.1 µM pyraclostrobin had no effect on mitochondrial respiration (Fig. 3B-F), while exposure to 1.0 and 10.0 µM pyraclostrobin had opposing effects. 1.0 µM pyraclostrobin increased basal oxygen consumption rate (OCR), ATP-linked respiration, maximal and spare respiratory capacity, and proton leak, while 10.0 µM pyraclostrobin reduced basal OCR, ATP-linked respiration, and maximal and spare respiratory capacity several-fold (Fig. 3B-F). Collectively, these results demonstrate a dose-dependent disruption of mitochondrial function resulting in ATP depletion, loss of mitochondrial membrane potential (Fig. S2), and TG accumulation.

In contrast to pyraclostrobin, 0.1 and 1.0 µM rosiglitazone dramatically increased basal OCR, ATP-linked respiration, and proton leak (Fig. 3B,C,F), while 0.01 µM rosiglitazone had no effect on mitochondrial respiration. Note that the maximal and spare respiratory capacity could not be accurately measured for rosiglitazone (0.1 & 1.0 µM) treated cells, as uncoupling mitochondrial respiration with FCCP resulted in a rapid (within ~30 seconds) depletion of oxygen within the Seahorse XF^e microchamber, which subjected the cells to anoxia. Given that 3T3-L1 preadipocytes must grow to confluency prior to differentiation, and that the minimal Seahorse XF^e measurement interval time is two minutes, this limitation could not be overcome. Representative Seahorse XF^e plots are shown in (Fig. S3).

3.3 Pyraclostrobin disrupts glucose and fatty acid metabolism.

In response to mitochondrial dysfunction cells can upregulate aerobic glycolysis to help maintain intracellular ATP levels. Furthermore, glycolytic intermediates can fuel lipogenesis, while the glycolytically-fueled pentose phosphate pathway can generate ribose-5-phosphate for nucleotide biosynthesis. Thus, an increase in glycolysis could generate the precursors required for TG accumulation and increased cell proliferation. To test for increased glucose metabolism, we measured expression of the glucose transporters, *Glut-1* and *Glut-4*, and phosphofructokinase (muscle (*Pfkm*) and liver (*Pfkl*) isoforms) and pyruvate kinase (muscle isoform (*Pkm*)), two enzymes that catalyze rate-limiting steps of glycolysis. Expression of *Glut-4*, *Pfkl*, *Pfkm*, and *Pkm* were downregulated in cells treated with pyraclostrobin (Fig. 4B-E), while a suggestive, but non-significant trend in increased *Glut-1* expression was measured in cells exposed to 10.0 µM pyraclostrobin (p=0.08 for post-hoc comparison to control; Fig. 4A). Alternatively, expression of *Glut-1*, *Glut-4*, *Pfkl*, *Pfkm*, and *Pkm* mRNA were increased in rosiglitazone treated cells (Fig. 4A-E).

To further test for increased glycolysis, we measured the rate at which cells acidified their media (also known as the extracellular acidification rate (ECAR)) using the Seahorse XF^e Bioanalyzer. ECAR provides an indirect measure of glycolysis, as excretion of glycolytic end products (i.e. lactate) results in acidification of the media. Consistent with an increase in glycolysis, ECAR was elevated in cells continuously exposed to pyraclostrobin (1.0 & 10.0 µM) and rosiglitazone (0.1 & 1.0 µM) (Fig. 5). Despite the discrepancy between ECAR and mRNA expression studies, ECAR provides a functional measure of glycolysis, while a lack of induction of glycolytic genes may be explained by the fact that many enzymes involved in glycolysis are regulated via post-translational modifications, allosterically regulated, or regulated via feedback or feedforward mechanisms (Chandel, 2015).

Finally, to investigate fatty acid metabolism, we measured expression of carnitine palmitoyltransferase 1 (*Cpt-1b* (muscle isoform)), an enzyme that facilitates the rate-limiting step in the transport of fatty acids into the mitochondrial matrix to undergo fatty acid oxidation. Pyraclostrobin decreased *Cpt-1b* expression, while rosiglitazone increased *Cpt-1b* expression (Fig. 6A). These results suggest that exposure to pyraclostrobin is reducing mitochondrial fatty acid oxidation. Furthermore, exposure to pyraclostrobin reduced expression of fatty acid synthase (*Fasn*), and acetyl-Coenzyme A carboxylase beta (*Acacb*) (Fig. 6B,D), suggesting a reduction in fatty acid synthesis via traditional lipogenesis mechanisms. Alternatively, exposure to rosiglitazone increased expression of *Fasn*, *Acaca*, and *Acacb* in a dose-dependent manner (Fig. 6B-D).

3.3 CREB plays a role in pyraclostrobin-induced TG accumulation.

cAMP responsive element binding protein (CREB) is a co-activator of PPARγ that is required to maximize adipogenesis and TG accumulation (Reusch *et al.*, 2000; Tang and Lane, 2012). Previously, it was shown that CREB activation was required for antimycin A, another ETC CIII inhibitor, induced TG-accumulation in 3T3-L1 cells in the absence of PPARγ activation (Vankoningsloo *et al.*, 2006). To test the role of CREB in pyraclostrobin-induced TG accumulation we co-exposed 3T3-L1 cells to pyraclostrobin and the CREB inhibitor 666-15 (Xie *et al.*, 2015). Inhibition of CREB reduced rosiglitazone-induced TG accumulation (Fig. 7). Furthermore, 666-15 also reduced pyraclostrobin-induced TG-accumulation in the absence of PPARγ activation (Fig. 7), demonstrating a role for CREB in pyraclostrobin-induced TG accumulation.

4. Discussion / Conclusions

Here, we have investigated how the high-production volume fungicide pyraclostrobin induces TG accumulation in 3T3-L1 cells, and report that TG accumulation is not associated with PPARγ activation, but instead is associated with a disruption of mitochondrial function and intermediary metabolism. Collectively, these results provide mechanistic insight into an emerging contaminant of human health concern that has been shown to disrupt lipid homeostasis in both murine (Kassotis *et al.*, 2017a) and human (Foley *et al.*, 2017) models of adipogenesis.

4.1 Pyraclostrobin-induced TG accumulation is independent of PPARγ activation.

Activation of the transcription factor PPARγ has been shown to be both necessary (Barak *et al.*, 1999; Kubota *et al.*, 1999; Rosen *et al.*, 1999) and sufficient (Hu *et al.*, 1995; Shao and Lazar, 1997; Tontonoz *et al.*, 1994) for normal adipogenesis; however, other transcription factors such as CREB, C/EBP, and ERRα, as well as other PPAR isoforms (PPARβ) are required to maximize adipogenesis (Matsusue *et al.*, 2004). Despite inducing a similar magnitude of TG accumulation as the PPARγ agonist rosiglitazone, pyraclostrobin did not act as a PPARγ agonist. Furthermore, exposure to pyraclostrobin reduced *PPARγ* and *Cebpα* mRNA expression, while also reducing the expression of lipoprotein lipase (*Lpl*), a gene transcriptionally regulated via PPARγ (Schoonjans *et al.*, 1996). Collectively, these results suggest pyraclostrobin is inducing TG accumulation through a mechanism independent of PPARγ activation in murine 3T3-L1 cells, which is further supported by the fact that exposure to two different PPARγ antagonists (GW9662, T0070907) did not mitigate pyraclostrobin-induced TG accumulation. Interestingly, it was recently demonstrated that pyraclostrobin can induce TG accumulation in a human adipose-derived stem cell model. In this model, siRNA knockdown of PPARγ partially mitigated TG accumulation suggesting the phenotype may be PPARγ-mediated (Foley *et al.*, 2017), potentially indicating species-specific differences in the mechanism underlying pyraclostrobin-induced TG

accumulation. However, and as discussed further below (section 4.2), pyraclostrobin appears to phenocopy our 3T3-L1 results in nearly every other metric tested, suggesting pyraclostrobin is having similar effects in human and murine models of adipogenesis.

4.2 Preadipocytes differentiated in the presence of pyraclostrobin lack many markers of mature adipocytes.

Preadipocytes differentiated for ten days in the presence of pyraclostrobin fail to express many common markers of adipocyte maturation, including *PPARγ*, *Cebpα*, and *Lpl*, suggesting pyraclostrobin is preventing differentiation. This is further supported by the fact that mature adipocytes treated with rosiglitazone display hypertrophia and a round shape, whereas pyraclostrobin-treated preadipocytes retain a fibroblast-like morphology. Similarly, pyraclostrobin was recently shown to limit the expression of many common markers of adipocyte maturation in a human adipose-derived stem cell model. In this study, pyraclostrobin treatment prevented expression of *Plin1* (mRNA) and *Fabp4* (mRNA and protein), secretion of adipokine, and only mildly induced *PPARγ* and *Cebpα* mRNA expression at a single concentration in a ten-point dose-response. Furthermore, a typical lipid accumulation phenotype (i.e. many small peripheral lipid droplets that coalesce into a large central lipid droplet that eventually displaces the nucleus) was not evident in pyraclostrobin treated cells. Collectively, these results suggest that pyraclostrobin may also prevent differentiation in human cells (Foley *et al.*, 2017).

Antimycin A, another ETC CIII inhibitor, has also been shown to prevent 3T3-L1 differentiation (Vankoningsloo *et al.*, 2005). Interestingly, it has been proposed that mitochondrial biogenesis may not only accompany adipogenesis, but may also precede and even be required for adipogenesis to occur. In the proposed model, an mTORC1-dependent increase in

mitochondrial biogenesis triggers a burst of mitochondrial ROS at ETC CIII, which is required to initiate PPARγ transcriptional activity and differentiation of primary human mesenchymal stem cells into adipocytes (Tormos *et al.*, 2011). These findings suggest proper mitochondrial function and biogenesis are not only required to help meet rising energy demands during adipogenesis, but also that low levels of mitochondrial ROS may serve as a signaling event required for the initiation of adipogenesis. This is further supported by the fact that elevated mitochondrial ROS has been implicated in various metabolic syndromes, including obesity and diabetes (Furukawa *et al.*, 2004; Houstis *et al.*, 2006). Given our rapidly expanding understanding of the role mitochondria play in adipogenesis, it is not surprising that mitochondrial toxicants such as antimycin A and pyraclostrobin may disrupt adipocyte differentiation.

4.3 Pyraclostrobin-induced mitochondrial dysfunction is associated with TG accumulation.

Given that pyraclostrobin is an ETC CIII inhibitor (Becker *et al.*, 1981), and the emerging role for mitochondria in adipogenesis [reviewed in (De Pauw *et al.*, 2009)], we hypothesized mitochondrial dysfunction may be underlying TG accumulation. In support of this, pyraclostrobin (1 and 10 µM) reduced both mitochondrial membrane potential and steady-state ATP levels; however, pyraclostrobin had opposing effects on mitochondrial respiration: exposure to 10 µM pyraclostrobin inhibited respiration, while 1 µM increased respiration. The increase in mitochondrial respiration in response to 1 µM pyraclostrobin may represent a compensatory response in which other complexes of the ETC increase their activity in an attempt to overcome incomplete CIII inhibition. In support of this, adaptive responses to ETC mutations or partial inhibition are well documented in the literature (Falk *et al.*, 2008; Morgan *et al.*, 2015; Pulliam *et al.*, 2014); however, further work is required to test this hypothesis.

Interestingly, it was previously demonstrated that continuous exposure to ETC complex I (rotenone), complex III (stimatellin, myxothiazol, antimycin A), and complex V (oligomycin A) inhibitors can also induce TG accumulation in 3T3-L1 cells (Vankoningsloo *et al.*, 2005). Furthermore, antimycin A phenocopied many of the effects observed for pyraclostrobin, including altered lipid droplets morphology (droplets were smaller and more numerous), depletion of ATP, a fibroblast-like cell morphology, and a lack of expression of many common markers of mature adipocytes (i.e. *Cebpα*, *PPARγ*, *Lpl* expression). Importantly, this phenotype occurred in the absence of PPARγ activation, suggesting TG accumulation was occurring through an alternative mechanism. Further mechanistic studies with antimycin A revealed a downregulation of lipogenesis and fatty acid oxidation, and an increase in GLUT4 expression and glucose uptake, while radiolabeling experiments revealed a direct glucose-to-TG conversion, suggesting glycolytic intermediates (i.e. dihydroxyacetone phosphate) were being converted to glycerol 3-phosphate to fuel the re-esterification of free fatty acids into TGs (Vankoningsloo *et al.*, 2005). This mechanism appears to be mediated by cAMP-response-element binding protein (CREB), a transcription factor known to regulate glucose and lipid metabolism (Herzig *et al.*, 2003; Zhou *et al.*, 2004), as antimycin A-induced mitochondrial dysfunction activated CREB, and CREB knockdown prevented TG accumulation (Vankoningsloo *et al.*, 2006).

Importantly, inhibiting CREB activity reduced pyraclostrobin-induced TG accumulation, suggesting pyraclostrobin and antimycin A are inducing TG accumulation through a similar CREB-driven mechanism. Furthermore, pyraclostrobin reduced expression of fatty acid oxidation (*Cpt-1b*) and lipogenic (*Fasn, Acacα, Acacβ*) genes, while an increase in ECAR suggests an increase in glucose metabolism. Although we did not see an induction of *Glut-4* expression after ten days of differentiation, antimycin A only induced *Glut-4* expression early in

the differentiation protocol (day 2), thus our study may have missed certain transcriptional changes. We propose a model (Fig. 8) in which either PPARγ activation or mitochondrial inhibition may lead to adipogenesis. Finally, it is important to note that antimycin A induces TG accumulation in 3T3-L1 cells at a 100-fold lower dose than pyraclostrobin (10 nM vs. 1 uM), raising the possibility that the concentrations of pyraclostrobin used in the present study, and their subsequent *in vitro* effects, are not representative of actual human exposure. However, human exposure to pyraclostrobin is not monitored, so there is a great deal of uncertainty surrounding exposure estimates. The active concentrations of pyraclostrobin used in the present study range from 388 ppb (1 µM) to 3.88 ppm (10 µM), while pyraclostrobin has been detected on a variety of human food products in the low ppm range (4-20 ppm) (Dong *et al.*, 2012; Guo *et al.*, 2017; Kovacova *et al.*, 2013; Pearson *et al.*, 2016); however, extrapolating the concentrations of pyraclostrobin used *in vitro* cannot be extrapolated to human exposure studies without knowing more about bioavailability, and *in vivo* effects. Furthermore, a recent human toxicity assessment estimated that oral exposure to pyraclostrobin exceeds the oral equivalent dose required to adversely affect mitochondrial function (Wetmore *et al.*, 2011). Collectively, these findings suggest human exposure to pyraclostrobin may be sufficient to adversely affect mitochondrial health; however, further *in vivo* work is necessary to better understand the potential human health effects of pyraclostrobin.

Acknowledgements: This work was supported by the National Institute of Health and the National Institute of Environmental Health Sciences [P42ES010356 to JNM, F31ES026859 to ALL, and R01 ES016099 to CDK and HMS].

References

Amuna, P., and Zotor, F. B. (2008). Epidemiological and nutrition transition in developing countries: impact on human health and development. *Proceedings of the Nutrition Society* **67**(01), 82-90.

Barak, Y., Nelson, M. C., Ong, E. S., Jones, Y. Z., Ruiz-Lozano, P., Chien, K. R., Koder, A., and Evans, R. M. (1999). PPAR gamma is required for placental, cardiac, and adipose tissue development. *Molecular cell* **4**(4), 585-95.

Battaglin, W. A., Sandstrom, M. W., Kuivila, K. M., Kolpin, D. W., and Meyer, M. T. (2011). Occurrence of azoxystrobin, propiconazole, and selected other fungicides in US streams, 2005–2006. *Water, Air, & Soil Pollution* **218**(1-4), 307-322.

Becker, W., Von Jagow, G., Anke, T., and Steglich, W. (1981). Oudemansin, strobilurin A, strobilurin B and myxothiazol: new inhibitors of the bc1 segment of the respiratory chain with an E-β-methoxyacrylate system as common structural element. *FEBS letters* **132**(2), 329-333.

Chandel, N. S. (2015). *Navigating metabolism*. Cold Spring Harbor Laboratory.

Dabelea, D., Mayer-Davis, E. J., Saydah, S., Imperatore, G., Linder, B., Divers, J., Bell, R., Badaru, A., Talton, J. W., and Crume, T. (2014). Prevalence of type 1 and type 2 diabetes among children and adolescents from 2001 to 2009. *Jama* **311**(17), 1778-1786.

Daval, M., Diot-Dupuy, F., Bazin, R., Hainault, I., Viollet, B., Vaulont, S., Hajduch, E., Ferré, P., and Foufelle, F. (2005). Anti-lipolytic action of AMP-activated protein kinase in rodent adipocytes. *Journal of Biological Chemistry* **280**(26), 25250-25257.

De Pauw, A., Tejerina, S., Raes, M., Keijer, J., and Arnould, T. (2009). Mitochondrial (dys)function in adipocyte (de)differentiation and systemic metabolic alterations. *The American journal of pathology* **175**(3), 927-39.

Dong, F., Chen, X., Liu, X., Xu, J., Li, Y., Shan, W., and Zheng, Y. (2012). Simultaneous determination of five pyrazole fungicides in cereals, vegetables and fruits using liquid chromatography/tandem mass spectrometry. *Journal of Chromatography A* **1262**, 98-106.

Falk, M., Zhang, Z., Rosenjack, J., Nissim, I., Daikhin, E., Sedensky, M. M., Yudkoff, M., and Morgan, P. G. (2008). Metabolic pathway profiling of mitochondrial respiratory chain mutants in C. elegans. *Molecular genetics and metabolism* **93**(4), 388-397.

Falutz, J. (2007). Therapy insight: body-shape changes and metabolic complications associated with HIV and highly active antiretroviral therapy. *Nature Reviews. Endocrinology* **3**(9), 651.

Fang, M., Webster, T. F., and Stapleton, H. M. (2015). Activation of human peroxisome proliferator-activated nuclear receptors (PPARγ1) by semi-volatile compounds (SVOCs) and chemical mixtures in indoor dust. *Environmental science & technology* **49**(16), 10057-10064.

Fassina, G., Dorigo, P., and Gaion, R. (1974). Equilibrium between metabolic pathways producing energy: a key factor in regulating lipolysis. *Pharmacological research communications* **6**(1), 1-21.

Foley, B., Doheny, D. L., Black, M. B., Pendse, S. N., Wetmore, B. A., Clewell, R. A., Andersen, M. E., and Deisenroth, C. (2017). Screening ToxCast Prioritized Chemicals for PPARG Function in a Human Adipose-Derived Stem Cell Model of Adipogenesis. *Toxicological sciences : an official journal of the Society of Toxicology* **155**(1), 85-100.

Forman, B. M., Tontonoz, P., Chen, J., Brun, R. P., Spiegelman, B. M., and Evans, R. M. (1995). 15-deoxy-Δ12, 14-prostaglandin J2 is a ligand for the adipocyte determination factor PPARγ. *Cell* **83**(5), 803-812.

Furukawa, S., Fujita, T., Shimabukuro, M., Iwaki, M., Yamada, Y., Nakajima, Y., Nakayama, O., Makishima, M., Matsuda, M., and Shimomura, I. (2004). Increased oxidative stress in obesity and its impact on metabolic syndrome. *The Journal of clinical investigation* **114**(12), 1752-1761.

Guo, X., Wu, W., Song, N., Li, J., Kong, D., Kong, X., He, J., Chen, K., and Shan, Z. (2017). Residue dynamics and risk assessment of pyraclostrobin in rice, plants, hulls, field soil, and paddy water. *Human and Ecological Risk Assessment: An International Journal* **23**(1), 67-81.

Hammond, R. A., and Levine, R. (2010). The economic impact of obesity in the United States. *Diabetes Metab Syndr Obes* **3**(1), 285-95.

Heilbronn, L. K., Gan, S. K., Turner, N., Campbell, L. V., and Chisholm, D. J. (2007). Markers of mitochondrial biogenesis and metabolism are lower in overweight and obese insulin-resistant subjects. *The Journal of Clinical Endocrinology & Metabolism* **92**(4), 1467-1473.

Herzig, S., Hedrick, S., Morantte, I., and Koo, S.-H. (2003). CREB controls hepatic lipid metabolism through nuclear hormone receptor PPAR-gama. *Nature* **426**(6963), 190.

Houstis, N., Rosen, E. D., and Lander, E. S. (2006). Reactive oxygen species have a causal role in multiple forms of insulin resistance. *Nature* **440**(7086), 944-948.

Hu, E., Tontonoz, P., and Spiegelman, B. M. (1995). Transdifferentiation of myoblasts by the adipogenic transcription factors PPAR gamma and C/EBP alpha. *Proceedings of the National Academy of Sciences of the United States of America* **92**(21), 9856-60.

Kassotis, C. D., Hoffman, K., and Stapleton, H. M. (2017a). Characterization of Adipogenic Activity of House Dust Extracts and Semi-Volatile Indoor Contaminants in 3T3-L1 Cells. *Environmental Science & Technology* doi: 10.1021/acs.est.7b01788.

Kassotis, C. D., Masse, L., Kim, S., Schlezinger, J. J., Webster, T. F., and Stapleton, H. M. (2017b). Characterization of Adipogenic Chemicals in Three Different Cell Culture Systems: Implications for Reproducibility Based on Cell Source and Handling. *Scientific Reports* **7**, 42104.

Kovacova, J., Hrbek, V., Kloutvorova, J., Kocourek, V., Drabova, L., and Hajslova, J. (2013). Assessment of pesticide residues in strawberries grown under various treatment regimes. *Food additives & contaminants. Part A, Chemistry, analysis, control, exposure & risk assessment* **30**(12), 2123-35.

Kubota, N., Terauchi, Y., Miki, H., Tamemoto, H., Yamauchi, T., Komeda, K., Satoh, S., Nakano, R., Ishii, C., and Sugiyama, T. (1999). PPARγ mediates high-fat diet–induced adipocyte hypertrophy and insulin resistance. *Molecular cell* **4**(4), 597-609.

Lefterova, M. I., Zhang, Y., Steger, D. J., Schupp, M., Schug, J., Cristancho, A., Feng, D., Zhuo, D., Stoeckert, C. J., Jr., Liu, X. S., *et al.* (2008). PPARgamma and C/EBP factors orchestrate adipocyte biology via adjacent binding on a genome-wide scale. *Genes & development* **22**(21), 2941-52.

Lehmann, J. M., Moore, L. B., Smith-Oliver, T. A., Wilkison, W. O., Willson, T. M., and Kliewer, S. A. (1995). An antidiabetic thiazolidinedione is a high affinity ligand for

peroxisome proliferator-activated receptor γ (PPARγ). *Journal of Biological Chemistry* **270**(22), 12953-12956.

Li, R.-j., Yu, J.-l., Song, G.-c., and Ma, H. (2010). Residue dynamics of pyraclostrobin in pyraclostrobin+ metiram in grape and soil. *Environmental Chemistry* **4**, 619-622.

Lowell, B. B., and Shulman, G. I. (2005). Mitochondrial dysfunction and type 2 diabetes. *Science* **307**(5708), 384-387.

Lozowicka, B., and Jankowska, M. (2016). Comparison of the effects of water and thermal processing on pesticide removal in selected fruit and vegetables. *Journal of Elementology* **21**(1).

Lozowicka, B., Jankowska, M., Hrynko, I., and Kaczynski, P. (2016). Removal of 16 pesticide residues from strawberries by washing with tap and ozone water, ultrasonic cleaning and boiling. *Environmental monitoring and assessment* **188**(1), 51.

Matsusue, K., Peters, J. M., and Gonzalez, F. J. (2004). PPARbeta/delta potentiates PPARgamma-stimulated adipocyte differentiation. *FASEB journal : official publication of the Federation of American Societies for Experimental Biology* **18**(12), 1477-9.

Morgan, P. G., Higdon, R., Kolker, N., Bauman, A., Ilkayeva, O., Newgard, C., Kolker, E., Steele, L., and Sedensky, M. M. (2015). Comparison of proteomic and metabolomic profiles of mutants of the mitochondrial respiratory chain in Caenorhabditis elegans. *Mitochondrion* **20**, 95-102.

Ogden, C. L., Carroll, M. D., and Flegal, K. M. (2014). Prevalence of obesity in the United States. *Jama* **312**(2), 189-190.

Oliver, R. P., and Hewitt, H. G. (2014). *Fungicides in crop protection*. 2 ed. CABI.

Pearson, B. L., Simon, J. M., McCoy, E. S., Salazar, G., Fragola, G., and Zylka, M. J. (2016). Identification of chemicals that mimic transcriptional changes associated with autism, brain aging and neurodegeneration. *Nature communications* **7**.

Petersen, K. F., Befroy, D., Dufour, S., Dziura, J., Ariyan, C., Rothman, D. L., DiPietro, L., Cline, G. W., and Shulman, G. I. (2003). Mitochondrial dysfunction in the elderly: possible role in insulin resistance. *Science* **300**(5622), 1140-1142.

Pettis, J. S., Lichtenberg, E. M., Andree, M., Stitzinger, J., and Rose, R. (2013). Crop pollination exposes honey bees to pesticides which alters their susceptibility to the gut pathogen Nosema ceranae. *PloS one* **8**(7), e70182.

Pulliam, D. A., Deepa, S. S., Liu, Y., Hill, S., Lin, A.-L., Bhattacharya, A., Shi, Y., Sloane, L., Viscomi, C., and Zeviani, M. (2014). Complex IV-deficient Surf1−/− mice initiate mitochondrial stress responses. *Biochemical Journal* **462**(2), 359-371.

Reusch, J. E., Colton, L. A., and Klemm, D. J. (2000). CREB activation induces adipogenesis in 3T3-L1 cells. *Molecular and cellular biology* **20**(3), 1008-20.

Rosen, E. D., Sarraf, P., Troy, A. E., Bradwin, G., Moore, K., Milstone, D. S., Spiegelman, B. M., and Mortensen, R. M. (1999). PPAR gamma is required for the differentiation of adipose tissue in vivo and in vitro. *Molecular cell* **4**(4), 611-7.

Schoonjans, K., Peinado-Onsurbe, J., Lefebvre, A. M., Heyman, R. A., Briggs, M., Deeb, S., Staels, B., and Auwerx, J. (1996). PPARalpha and PPARgamma activators direct a distinct tissue-specific transcriptional response via a PPRE in the lipoprotein lipase gene. *The EMBO journal* **15**(19), 5336-48.

Semple, R., Crowley, V., Sewter, C., Laudes, M., Christodoulides, C., Considine, R., Vidal-Puig, A., and O'rahilly, S. (2004). Expression of the thermogenic nuclear hormone receptor

coactivator PGC-1α is reduced in the adipose tissue of morbidly obese subjects. *International journal of obesity* **28**(1), 176-179.

Shao, D., and Lazar, M. A. (1997). Peroxisome proliferator activated receptor γ, CCAAT/enhancer-binding protein α, and cell cycle status regulate the commitment to adipocyte differentiation. *Journal of Biological Chemistry* **272**(34), 21473-21478.

Spiegelman, B., Puigserver, P., and Wu, Z. (2000). Regulation of adipogenesis and energy balance by PPAR [gamma] and PGC-1. *International Journal of Obesity* **24**(S4), S8.

Tang, Q. Q., and Lane, M. D. (2012). Adipogenesis: from stem cell to adipocyte. *Annual review of biochemistry* **81**, 715-736.

Tontonoz, P., Hu, E., and Spiegelman, B. M. (1994). Stimulation of adipogenesis in fibroblasts by PPARγ2, a lipid-activated transcription factor. *Cell* **79**(7), 1147-1156.

Tormos, K. V., Anso, E., Hamanaka, R. B., Eisenbart, J., Joseph, J., Kalyanaraman, B., and Chandel, N. S. (2011). Mitochondrial complex III ROS regulate adipocyte differentiation. *Cell metabolism* **14**(4), 537-544.

USGS (2017). *Estimated Annual Agricultural Pesticide Use.* Available at: https://water.usgs.gov/nawqa/pnsp/usage/maps/show_map.php?year=2014&map=PYRACLOSTROBIN&hilo=L&disp=Pyraclostrobin. Accessed May 18, 2017.

Vankoningsloo, S., De Pauw, A., Houbion, A., Tejerina, S., Demazy, C., de Longueville, F., Bertholet, V., Renard, P., Remacle, J., Holvoet, P., *et al.* (2006). CREB activation induced by mitochondrial dysfunction triggers triglyceride accumulation in 3T3-L1 preadipocytes. *Journal of cell science* **119**(Pt 7), 1266-82.

Vankoningsloo, S., Piens, M., Lecocq, C., Gilson, A., De Pauw, A., Renard, P., Demazy, C., Houbion, A., Raes, M., and Arnould, T. (2005). Mitochondrial dysfunction induces

triglyceride accumulation in 3T3-L1 cells: role of fatty acid beta-oxidation and glucose. *Journal of lipid research* **46**(6), 1133-49.

Wetmore, B. A., Wambaugh, J. F., Ferguson, S. S., Sochaski, M. A., Rotroff, D. M., Freeman, K., Clewell III, H. J., Dix, D. J., Andersen, M. E., and Houck, K. A. (2011). Integration of dosimetry, exposure, and high-throughput screening data in chemical toxicity assessment. *Toxicological Sciences* **125**(1), 157-174.

Wilson-Fritch, L., Burkart, A., Bell, G., Mendelson, K., Leszyk, J., Nicoloro, S., Czech, M., and Corvera, S. (2003). Mitochondrial biogenesis and remodeling during adipogenesis and in response to the insulin sensitizer rosiglitazone. *Molecular and cellular biology* **23**(3), 1085-94.

Wilson-Fritch, L., Nicoloro, S., Chouinard, M., Lazar, M. A., Chui, P. C., Leszyk, J., Straubhaar, J., Czech, M. P., and Corvera, S. (2004). Mitochondrial remodeling in adipose tissue associated with obesity and treatment with rosiglitazone. *The Journal of clinical investigation* **114**(9), 1281-9.

Xie, F., Li, B. X., Kassenbrock, A., Xue, C., Wang, X., Qian, D. Z., Sears, R. C., and Xiao, X. (2015). Identification of a Potent Inhibitor of CREB-Mediated Gene Transcription with Efficacious in Vivo Anticancer Activity. *Journal of Medicinal Chemistry* **58**(12), 5075-5087.

You, X., Liu, C., Liu, F., Liu, Y., and Dong, J. (2012). Dissipation of pyraclostrobin and its metabolite BF-500-3 in maize under field conditions. *Ecotoxicology and environmental safety* **80**, 252-257.

Zhang, Z.-h., Li, H.-y., Wu, M., Yuan, Y.-w., Hu, X.-q., and Zheng, W.-r. (2009). Residue and risk assessment of chlorothalonil, myclobutanil and pyraclostrobin in greenhouse strawberry. *Chinese Journal of Pesticide Science* **4**, 010.

Zhou, X. Y., Shibusawa, N., Naik, K., Porras, D., Temple, K., Ou, H., Kaihara, K., Roe, M. W., Brady, M. J., and Wondisford, F. E. (2004). Insulin regulation of hepatic gluconeogenesis through phosphorylation of CREB-binding protein. *Nature medicine* **10**(6), 633.

Figure 1. Representative images of pyraclostrobin-induced triglyceride accumulation in 3T3-L1 cells. Lipid and DNA content is visualized with AdipoRed and NucBlue staining, respectively, in Zenbio 3T3-L1 cells differentiated according to standard protocols for ten days in the presence of 0.1% DMSO (vehicle control), or various concentrations of rosiglitazone or pyraclostrobin. Bright-field images were merged with a DAPI filter (to visualize NucBlue, blue) and a Green Fluorescent Protein filter (AdipoRed, green). Quantitative determination of lipid accumulation is shown in Fig. S1.

Figure 2. Pyraclostrobin-induced TG accumulation is independent of PPARγ activity. (A) Rosiglitazone (RSG) (one-way ANOVA ($p<0.0001$), N=4), but not pyraclostrobin (PYRA) (one-way ANOVA ($p=0.89$), N=4), increased PPARγ activity in a dose-dependent manner utilizing the Invitrogen GeneBLAzer PPARγ FRET reporter assay. Exposure to pyraclostrobin reduced (B) *PPARγ* (one-way ANOVA ($p<0.0001$), N=6), (C) *Cebpα* (transcription factor that regulates adipogenesis; one-way ANOVA ($p<0.0001$), N=6), and (D) *Lpl* (adipocyte marker; one-way ANOVA ($p<0.0001$), N=6) mRNA expression, while rosiglitazone increased the expression of all genes in Zenbio 3T3-L1 cells after ten days of differentiation. (E) The PPARγ antagonists GW9662 and T0070907 reduce RSG-induced TG accumulation (one-way ANOVA ($p=0.02$), N=3), while having no effect on PYRA-induced TG accumulation (one-way ANOVA ($p=0.38$), N=3). Asterisk denotes statistical significance ($p<0.05$) for post-hoc comparison (Dunnett's test) to control. Bars±SEM.

Figure 3. Exposure to pyraclostrobin causes mitochondrial dysfunction. (A) Continuous exposure to pyraclostrobin (PYRA) throughout a ten-day differentiation protocol reduced steady-state ATP levels in Zenbio 3T3-L1 cells (one-way ANOVA ($p<0.0001$), N=3). Interestingly, 1.0 and 10.0 µM pyraclostrobin had opposing effects (increased (1.0 µM) or decreased (10 µM)) on (B) basal oxygen consumption rate (OCR; one-way ANOVA ($p<0.0001$), N=15), (C) ATP-linked OCR (a measure of the amount of oxygen consumption directly linked to ATP-production; one-way ANOVA ($p<0.0001$), N=15), (D) maximal OCR (a measure of the maximum rate at which mitochondria can function; one-way ANOVA ($p<0.0001$), N=15), (E) spare respiratory capacity (maximal OCR - basal OCR; one-way ANOVA ($p<0.0001$), N=15), and (F) proton leak (transport of protons across the inner mitochondrial membrane independent of ATP synthase activity; one-way ANOVA ($p<0.0001$), N=15). Asterisk denotes statistical significance ($p<0.05$) for post-hoc comparison (Dunnett's test) to control. Bars±SEM. [1]Maximal and spare respiratory capacity could not be accurately measured for cells treated with 0.1 and 1.0 µM rosiglitazone (RSG), as cells rapidly depleted oxygen from the Seahorse XF^e microchamber resulting in anoxia.

Figure 4. Genes involved in glucose metabolism are down regulated following pyraclostrobin exposure. Continuous exposure to pyraclostrobin (PYRA) over the course of differentiation in Zenbio 3T3-L1 cells, and assessed ten days after induction, had no effect on mRNA expression of (A) *Glut-1* (one-way ANOVA ($p<0.0001$)), while expression of (B) *Glut-4* (one-way ANOVA ($p<0.0001$)), (C) *Pkm* (muscle isoform; involved in glycolysis; one-way ANOVA ($p<0.0001$)), (D) *Pfkm* (muscle isoform; involved in glycolysis; one-way ANOVA ($p<0.0001$)), and (E) *Pfkl* (liver isoform; involved in glycolysis; one-way ANOVA ($p<0.0001$))

were all down regulated. Alternatively, expression of all glucose transport and glycolysis genes were upregulated in response to rosiglitazone (RSG). Asterisk denotes statistical significance ($p<0.05$) for post-hoc comparison (Dunnett's test) to control. N=6. Bars±SEM.

Figure 5. Pyraclostrobin increased the extracellular acidification rate. Continuous exposure to pyraclostrobin (PYRA) or rosiglitazone (RSG) increased the extracellular acidification rate (ECAR), an indirect measure of glycolysis, of Zenbio 3T3-L1 cells (one-way ANOVA, $p<0.0001$) after ten days of differentiation. Asterisk denotes statistical significance ($p<0.05$) for post-hoc comparison (Dunnett's test) to control. Bars±SEM. N=15.

Figure 6. Genes involved in fatty acid metabolism are down regulated by pyraclostrobin. Exposure to pyraclostrobin (PYRA) over the course of a ten-day induction of differentiation in Zenbio 3T3-L1 cells decreased expression of (A) mitochondrial *Cpt-1b* (fatty acid oxidation gene; one-way ANOVA ($p<0.0001$)), (B) *Fasn* (fatty acid synthesis gene; one-way ANOVA ($p<0.0001$)), and (C) *Acacα* (fatty acid synthesis gene; one-way ANOVA ($p<0.0001$)) and (D) *Acacβ* (fatty acid synthesis gene; one-way ANOVA ($p<0.0001$)). Alternatively, expression of all fatty acid oxidation and synthesis genes were upregulated in response to rosiglitazone (RSG). Asterisk denotes statistical significance ($p<0.05$) for post-hoc comparison (Dunnett's test) to control. N=6. Bars±SEM.

Figure 7. CREB plays a role in pyraclostrobin-induced TG accumulation. Inhibiting CREB activity with 5 μM 666-15 reduced rosiglitazone (one-way ANOVA ($p=0.048$)) and pyraclostrobin (one-way ANOVA ($p=0.006$))-induced TG accumulation. Data is shown as %

control of TG accumulation in pyraclostrobin or rosiglitazone treated cells. Asterisk denotes statistical significance ($p<0.05$) for post-hoc comparison (Dunnett's test) to control. N=3. Bars±SEM.

Figure 8. Canonical and proposed non-canonical pathways of triglyceride accumulation. (A) Upon agonist binding, PPARγ, in cooperation with its co-activators (i.e. PGC1α, CREB, Cebpα, RXR), binds to the promoter region of target genes and induces transcriptional changes that facilitate adipocyte differentiation and maturation, TG accumulation, and mitochondrial biogenesis. Mitochondrial retrograde signaling is also depicted, as recent evidence suggests mitochondrial signaling may play a role in adipocyte differentiation (Tormos *et al.*, 2011). (B) Exposure to the electron transport chain inhibitor, antimycin A (AA), causes mitochondrial dysfunction that triggers CREB activation, while inhibiting adipocyte differentiation, PPARγ activation, FAO, and lipogenesis through traditional mechanisms (i.e. through the fatty acid synthase complex). CREB, a transcriptional regulator of lipid and glucose metabolism, promotes increased glucose uptake (via GLUT4) and glycolysis. The glycolytic intermediate, DHAP, can then be converted to G3P and used to fuel the re-esterification of free fatty acids (FFAs) resulting in TG formation and accumulation. Please note, pyruvate and Krebs cycle intermediates can also be used to generate G3P through a process known as glyceroneogenesis; however, radiolabeled glucose experiments suggest a direct glucose-to-TG conversion (Vankoningsloo *et al.*, 2005). Given that pyraclostrobin and AA are both complex III inhibitors that induce similar phenotypes in 3T3-L1 cells, it is plausible that pyraclostrobin is inducing TG accumulation through a similar mechanism. Abbreviations: Cebpα, CCAAT/ enhancer binding protein alpha; CREB, cAMP responsive element binding protein; DHAP, dihydroxyacetone phosphate; FAO, fatty acid β-

oxidation; G3P, glycerol 3-phosphate; GLUT4, glucose transporter 4; MMP, mitochondrial membrane potential; OXPHOS, oxidative phosphorylation; PPARg, peroxisome proliferator activated nuclear receptor gamma; PCG1α, PPARg coactivator 1-alpha; RXR, retinoid X receptor.

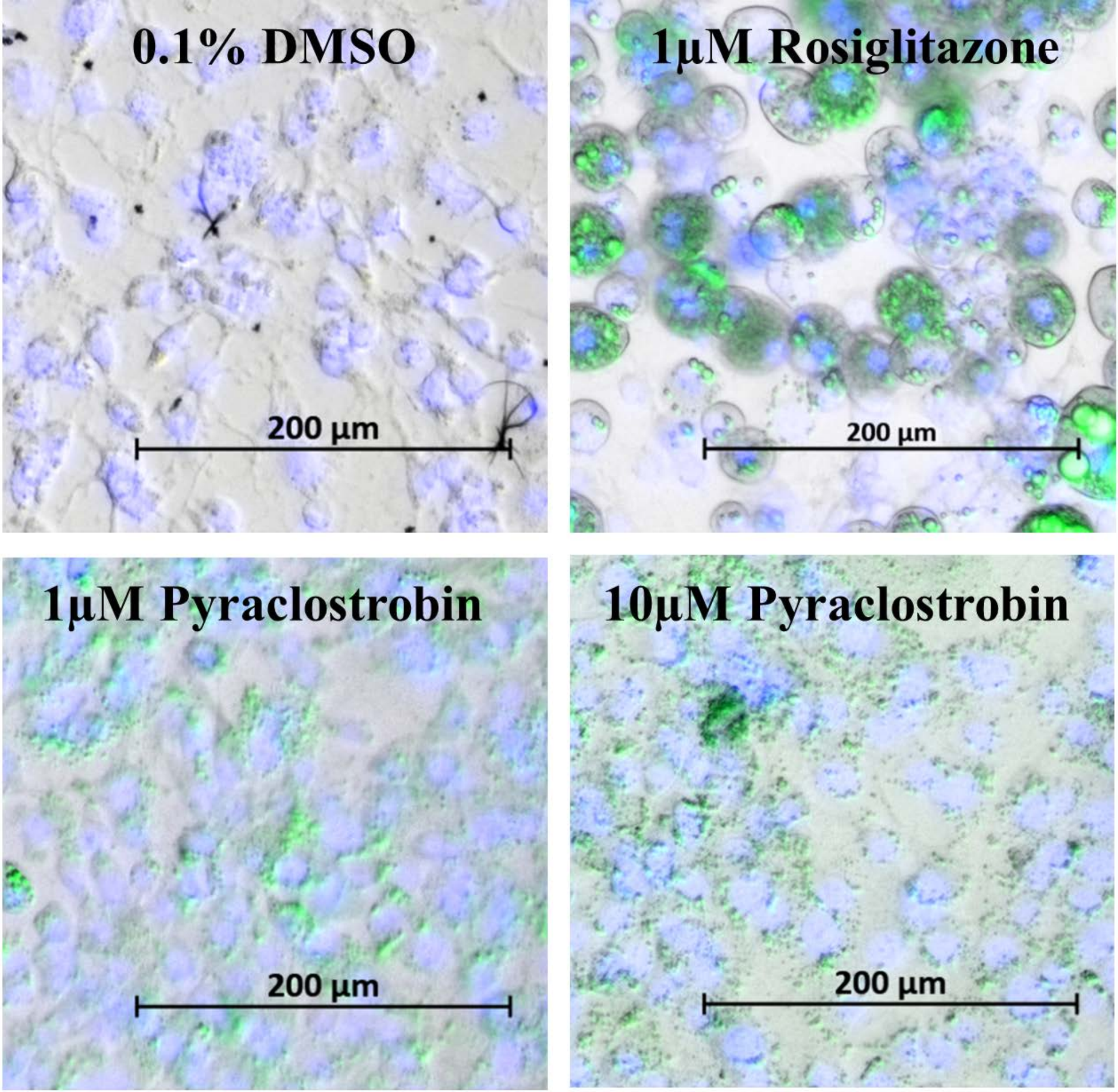
0.1% DMSO
200 µm
1µM Rosiglitazone
200 µm
1µM Pyraclostrobin
200 µm
10µM Pyraclostrobin
200 µm

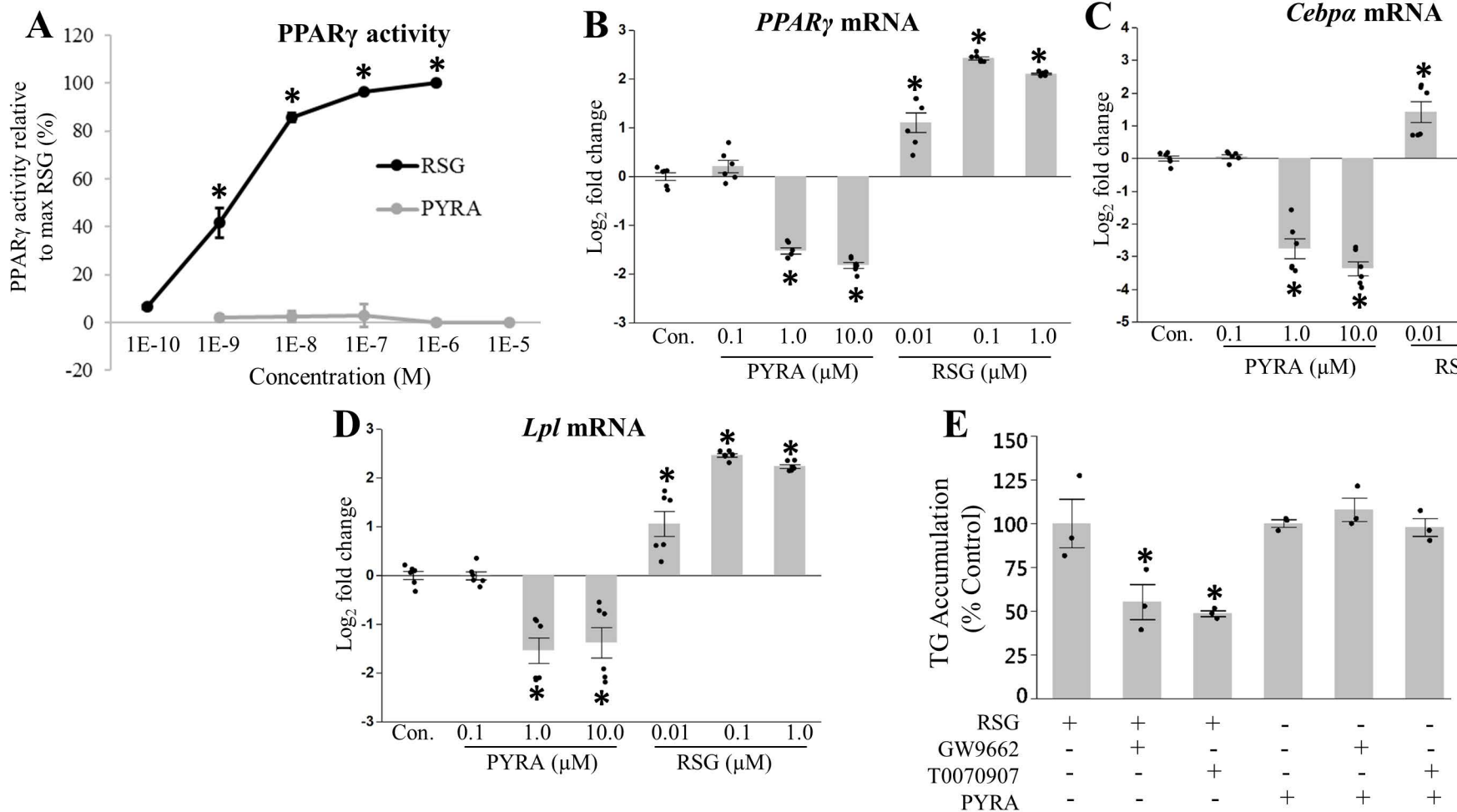
A
PPARγ activity
PPARγ activity relative to max RSG (%)
120
100
80
60
40
20
0
-20
RSG
PYRA
1E-10
1E-9
1E-8
1E-7
1E-6
1E-5
Concentration (M)
B
PPARγ mRNA
Log2 fold change
3
2
1
0
-1
-2
-3
Con.
0.1
1.0
10.0
0.01
0.1
1.0
PYRA (μM)
RSG (μM)
C
Cebpα mRNA
Log2 fold change
4
3
2
1
0
-1
-2
-3
-4
-5
Con.
0.1
1.0
10.0
0.01
0.1
1.0
PYRA (μM)
RSG (μM)
D
Lpl mRNA
Log2 fold change
3
2
1
0
-1
-2
-3
Con.
0.1
1.0
10.0
0.01
0.1
1.0
PYRA (μM)
RSG (μM)
E
TG Accumulation (% Control)
150
125
100
75
50
25
0
RSG + + + - - -
GW9662 - + - - + -
T0070907 - - + - - +
PYRA - - - + + +

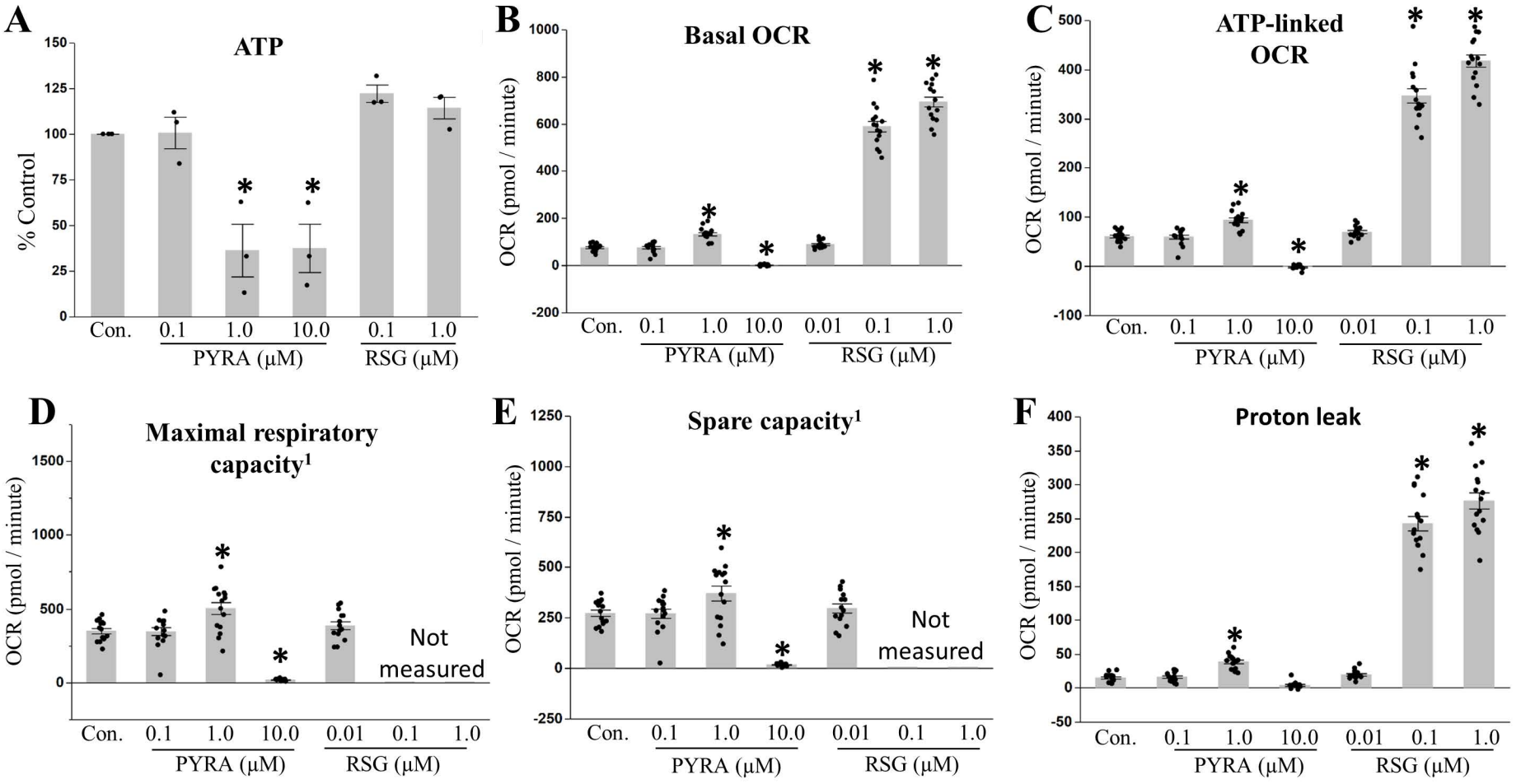
A
ATP
% Control
150
125
100
75
50
25
0
Con.
0.1
1.0
10.0
0.1
1.0
PYRA (μM)
RSG (μM)
B
Basal OCR
OCR (pmol / minute)
1000
800
600
400
200
0
-200
Con.
0.1
1.0
10.0
0.01
0.1
1.0
PYRA (μM)
RSG (μM)
C
ATP-linked OCR
OCR (pmol / minute)
500
400
300
200
100
0
-100
Con.
0.1
1.0
10.0
0.01
0.1
1.0
PYRA (μM)
RSG (μM)
D
Maximal respiratory capacity[1]
OCR (pmol / minute)
1500
1000
500
0
Not measured
Con.
0.1
1.0
10.0
0.01
0.1
1.0
PYRA (μM)
RSG (μM)
E
Spare capacity[1]
OCR (pmol / minute)
1250
1000
750
500
250
0
-250
Not measured
Con.
0.1
1.0
10.0
0.01
0.1
1.0
PYRA (μM)
RSG (μM)
F
Proton leak
OCR (pmol / minute)
400
350
300
250
200
150
100
50
0
-50
Con.
0.1
1.0
10.0
0.01
0.1
1.0
PYRA (μM)
RSG (μM)

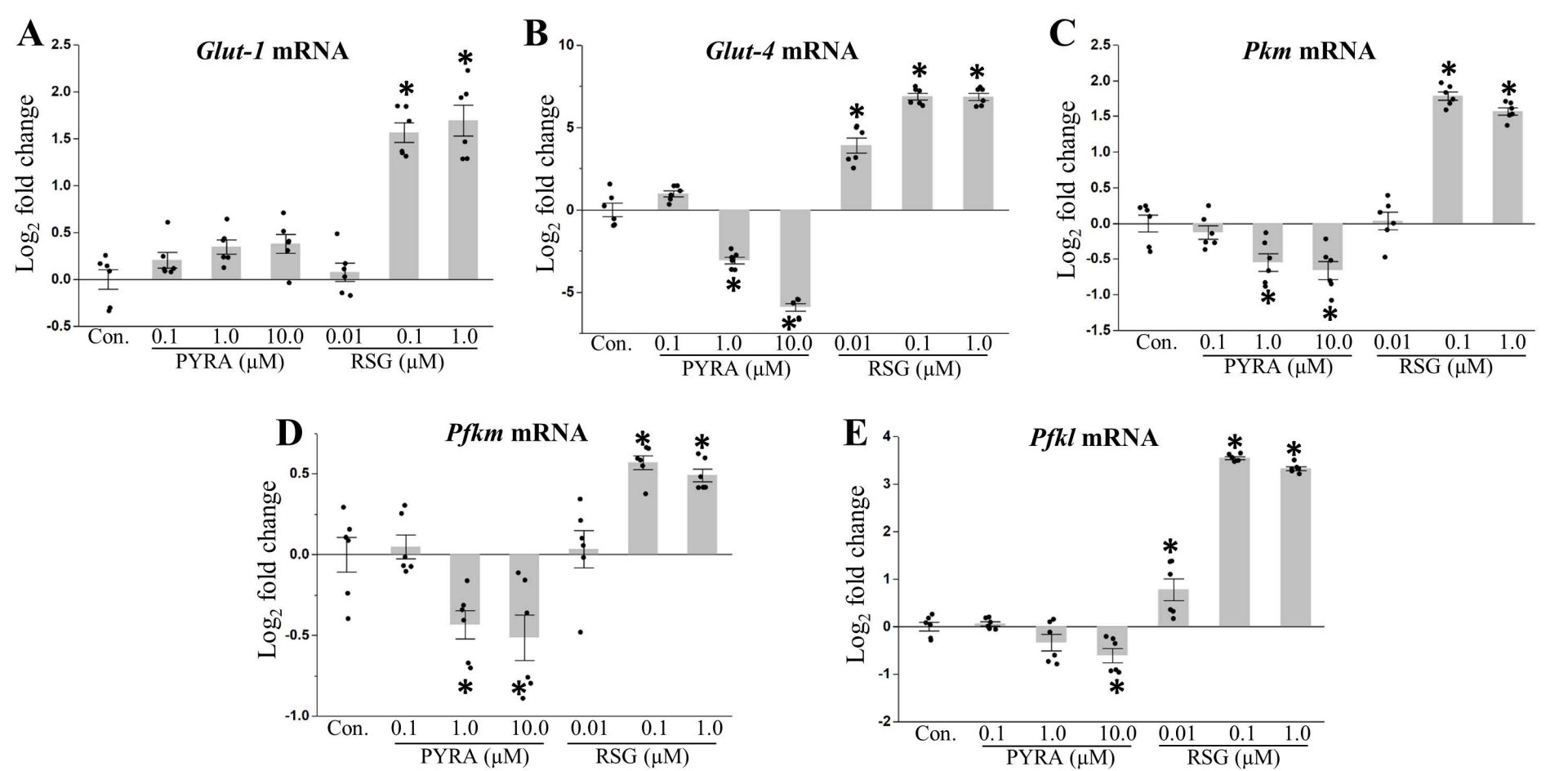
A
Glut-1 mRNA
Log2 fold change
Con.
0.1
1.0
10.0
0.01
0.1
1.0
PYRA (μM)
RSG (μM)
B
Glut-4 mRNA
C
Pkm mRNA
D
Pfkm mRNA
E
Pfkl mRNA

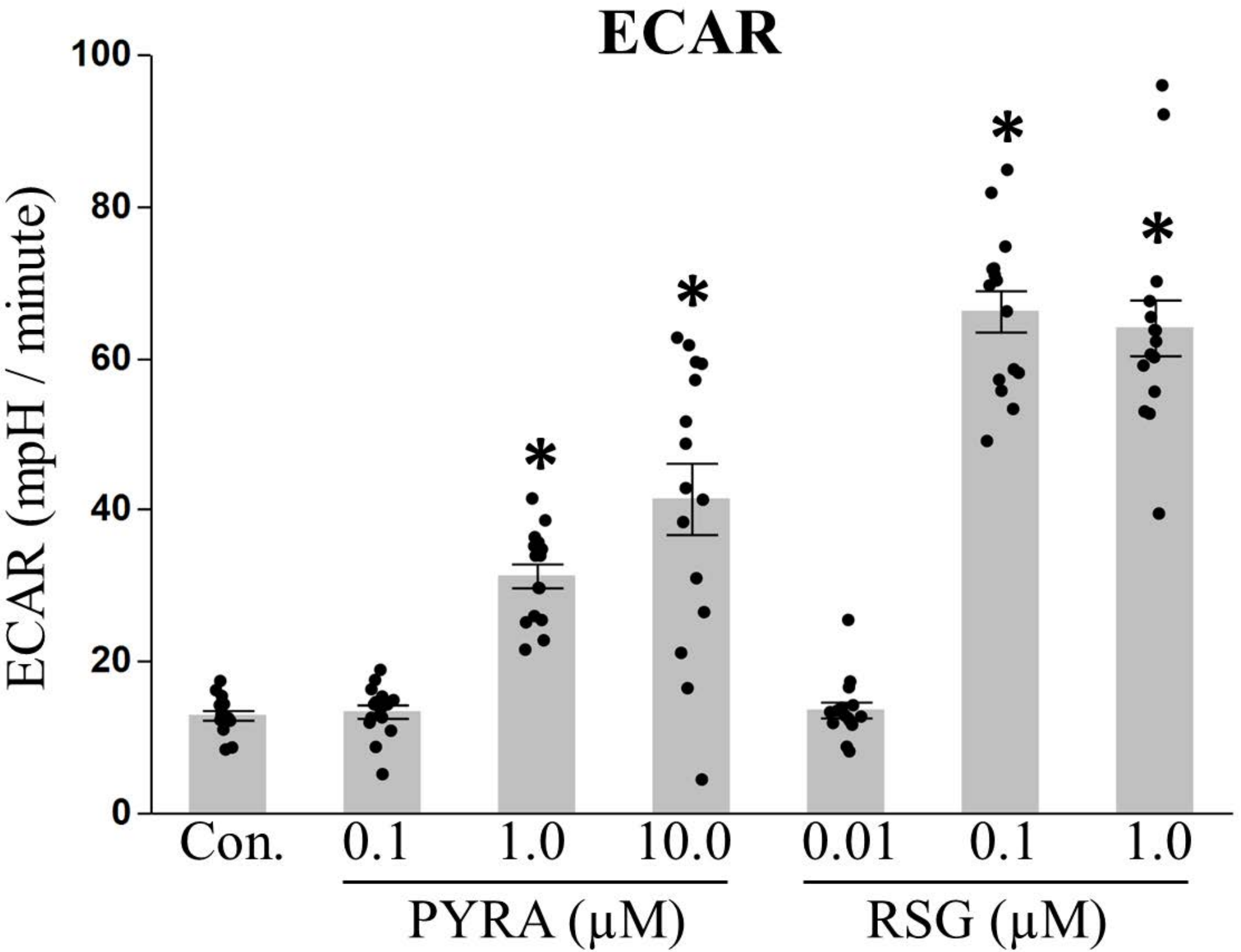
ECAR
ECAR (mpH / minute)
100
80
60
40
20
0
Con.
0.1
1.0
10.0
0.01
0.1
1.0
PYRA (μM)
RSG (μM)
*
*
*
*

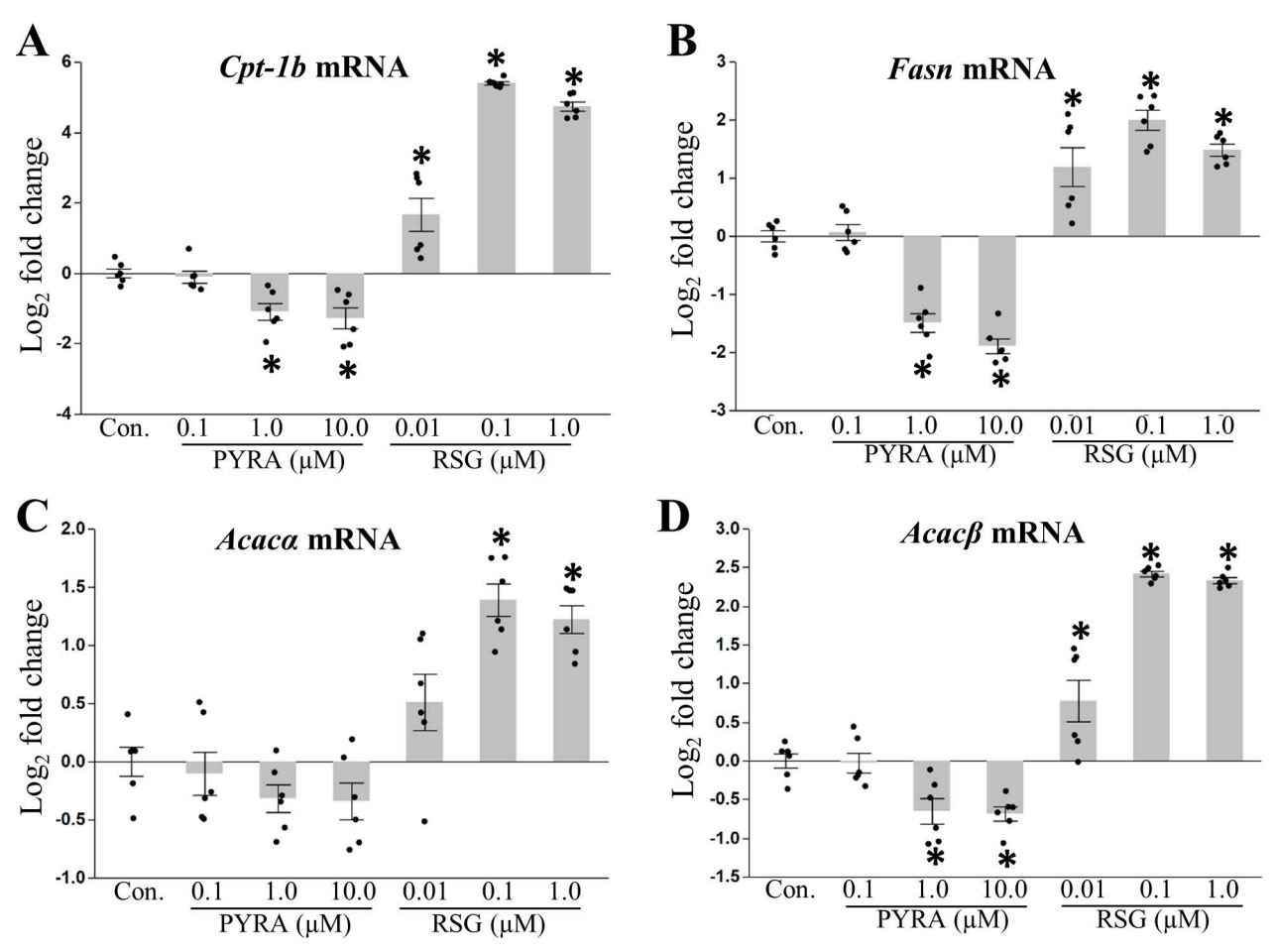
A
Cpt-1b mRNA
Log2 fold change
6
4
2
0
-2
-4
Con.
0.1
1.0
10.0
0.01
0.1
1.0
PYRA (μM)
RSG (μM)
B
Fasn mRNA
Log2 fold change
3
2
1
0
-1
-2
-3
Con.
0.1
1.0
10.0
0.01
0.1
1.0
PYRA (μM)
RSG (μM)
C
Acacα mRNA
Log2 fold change
2.0
1.5
1.0
0.5
0.0
-0.5
-1.0
Con.
0.1
1.0
10.0
0.01
0.1
1.0
PYRA (μM)
RSG (μM)
D
Acacβ mRNA
Log2 fold change
3.0
2.5
2.0
1.5
1.0
0.5
0.0
-0.5
-1.0
-1.5
Con.
0.1
1.0
10.0
0.01
0.1
1.0
PYRA (μM)
RSG (μM)

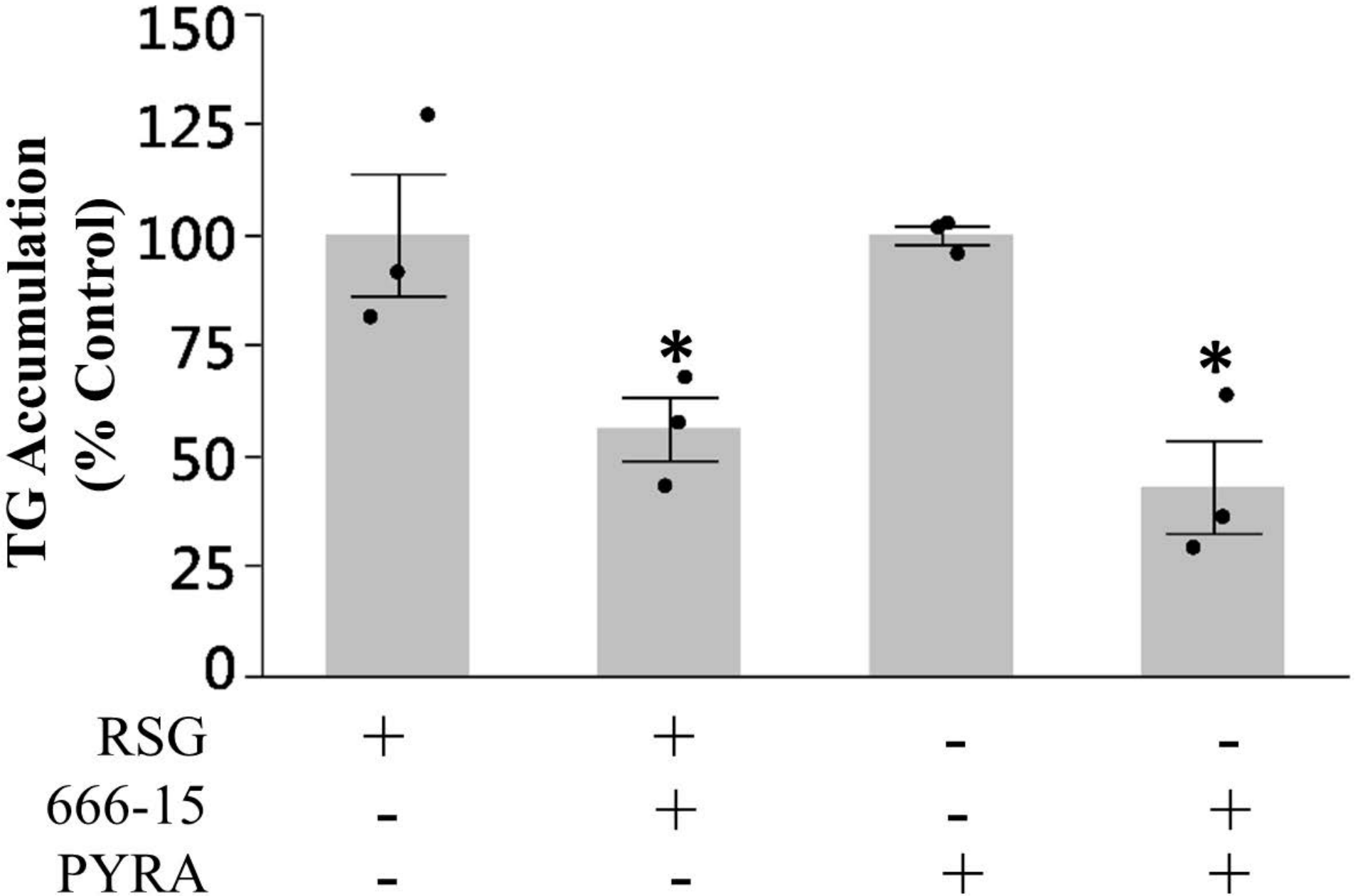
TG Accumulation
(% Control)
150
125
100
75
50
25
0
*
*
RSG + + - -
666-15 - + - +
PYRA - - + +

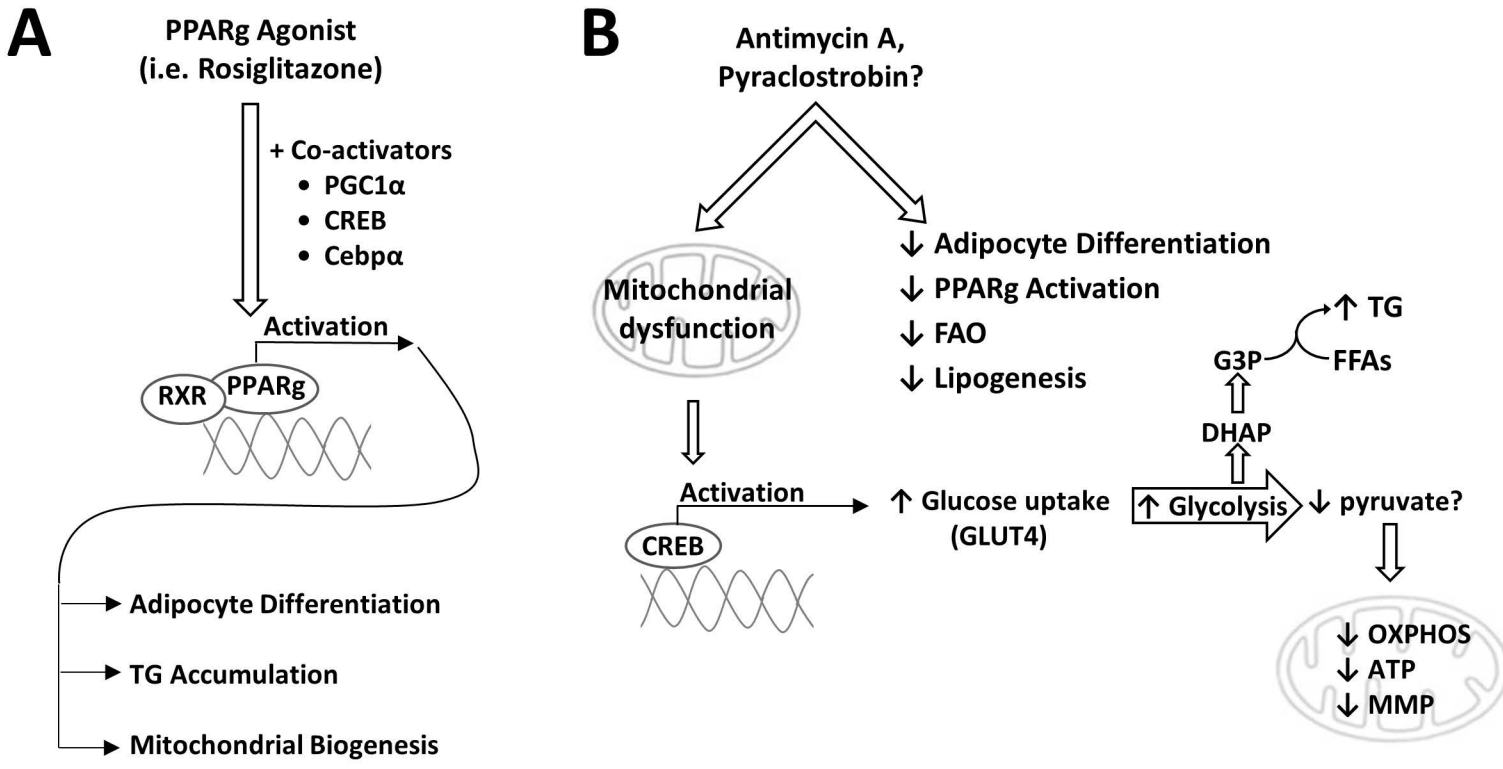
A
PPARg Agonist
(i.e. Rosiglitazone)
+ Co-activators
• PGC1α
• CREB
• Cebpα
Activation
RXR
PPARg
Adipocyte Differentiation
TG Accumulation
Mitochondrial Biogenesis
B
Antimycin A,
Pyraclostrobin?
Mitochondrial
dysfunction
↓ Adipocyte Differentiation
↓ PPARg Activation
↓ FAO
↓ Lipogenesis
Activation
CREB
↑ Glucose uptake
(GLUT4)
↑ Glycolysis
↓ pyruvate?
DHAP
G3P
↑ TG
FFAs
↓ OXPHOS
↓ ATP
↓ MMP